Pergamon

Int. J. Solids Structures Vol. 31, No. 19, pp. 2653–2677, 1994

0020–7683/94 $7.00 + .00

0020–7683(94)E0044–V

RESIDUAL STRESS EVOLUTION DUE TO COOL DOWN IN VISCOPLASTIC METAL MATRIX COMPOSITES

G. S. JEONG, D. H. ALLEN and D. C. LAGOUDAS
Center for Mechanics of Composites, Texas A and M University, College Station, TX 77843-3141, U.S.A.

(*Received* 1 *September* 1993; *in revised form* 14 *March* 1994)

Abstract—Two issues are considered in the current paper: (1) the effect of cool down from processing temperature on the thermally induced residual stresses in a representative volume element (RVE) of a periodic continuous fiber metal matrix composite monolayer; (2) the initiation of microcracks due to subsequent mechanical loading. A nonlinear incremental finite element program that accounts for thermoviscoplasticity in the matrix is utilized for the micromechanical analysis. The uncoupled heat conduction equation is solved for the spatial temperature distribution in the RVE for given cooling rates. Results indicate that spatial thermal gradients can induce significant stresses at rapid cooling rates. Furthermore, comparisons between thermoelastic and thermoviscoplastic predictions of residual stresses at the interface between the fiber and the matrix demonstrate that incorporating viscoplasticity may be significant in predicting certain damage mechanisms such as interfacial and radial matrix cracking. Finally, average stress–strain curves are obtained for the cases of mechanical loading with or without residual stresses, and predictions are made for the location and time at which interface debonding initiates.

1. INTRODUCTION

Metal matrix composites (MMCs) have the potential for high temperature use in place of heavier high temperature monolithic materials, such as metallic superalloys, in gas turbines and hypersonic flight structures. However, there are reliability concerns which need to be addressed. It has become apparent that the interface between fiber and matrix plays a profound role in the behavior of MMCs. The basic load transfer mechanism between fiber and matrix is dependent on a strong interfacial bond. Furthermore, the interface plays a very important role in the macroscopic ductility of a composite material because the energy dissipation due to sliding and debonding can increase effective resistance to further crack extension.

In MMCs at elevated temperatures, inelasticity in the matrix material introduces another level of complexity to the problem. In a metallic material under load at low homologous temperature, microstructural inelastic deformations occur primarily due to rate independent dislocation glide. At higher temperatures, thermally activated diffusional mechanisms cause the response to be rate dependent. Mechanisms may include dislocation climb and cross-slip, as well as phase changes and grain boundary creep and sliding. This inelasticity in the matrix can significantly affect residual stresses caused by cooling down from the processing temperature. Since the composite interface response is strongly dependent upon these residual stresses, it is important that micromechanical analyses include viscoplasticity.

The inelastic behavior of MMCs has been modeled utilizing computational schemes by several researchers. For example, Aboudi (1980) proposed an analytic model known as the method of cells. In this model, the composite is represented by a periodic rectangular array of cells and subcells. By imposing continuity of tractions between subcells and adjacent cells in an average sense, the approximate stress–strain behavior of the composite is obtained. This model has been used to predict the effective response of a continuous fiber elastoplastic metal matrix composite with residual stresses by Herakovich *et al.* (1990).

Sun *et al.* (1990) developed another micromechanical model assuming elastic fiber and elastic–plastic matrix. As was done in Aboudi's method of cells, a square array of fiber distribution was assumed. The fiber–matrix interfacial bond strength was estimated from the micromechanical model. A macromechanical model was used to characterize the constitutive behavior of the composite using a one-parameter plastic potential function. Thermal residual stresses were also estimated in the analysis.

Teply and Dvorak (1988) developed a periodic hexagonal array model to describe the effective response of MMCs with transversely isotropic properties. In particular, they used their model to derive bounds on the overall instantaneous properties of a fibrous B-Al system. The stresses in uncoated and coated fiber reinforced intermetallic matrix composites have been studied by Bahei-El-Din and Dvorak (1991). Various hot isostatic pressing (HIP) conditions were simulated by changing the processing temperature and pressure. The fiber and carbon coating were assumed to be elastic and the matrix was assumed to be elastic–plastic.

Using a generalized plane strain finite element analysis, Wisnom (1990) considered the effect on transverse tensile strength of fiber packing geometry, fiber spacing, residual stresses, interface strengths and matrix plasticity. The fiber–matrix interface was modeled using a spring element [see e.g. Benveniste (1985)]. A quadratic interaction criterion was adopted for the case where both tensile and shear stresses are significant. It was found that the interface strength is the most significant parameter. Residual stresses are beneficial, these being largely controlled by the yield strength of the matrix material at the time the residual stresses are set up. Fiber packing–spacing and matrix strength do not significantly affect the transverse strength of the composite.

Two-dimensional axisymmetric elements together with 20 node brick elements were used by Sherwood and Boyle (1990) to investigate the residual stress field which leads to interface cracking during cool down. A cyclic thermal load followed by a cyclic mechanical load at constant temperature was simulated.

Zywicz and Parks (1988) proposed a three-dimensional thermoviscoplastic modeling approach, based on the behavior of the individual constituents, in order to estimate the stresses which arise during manufacturing of an MMC. It was shown that fiber volume fraction and cooling rates affect the residual stresses. Damage was not considered.

A viscoplastic finite element analysis in which the response of whisker-reinforced aluminum composite subjected to longitudinal loading was studied by Povirk *et al.* (1991). In this analysis, decohesion of the whisker ends was assumed to be the dominant failure mode. They predicted the effects of both thermal residual stresses and whisker spacing on the average stress–strain response of the composite. The heat equation, with a coupling term due to the heat generated by plastic deformation, and the equilibrium equations were solved simultaneously.

In a recent work, Jeong *et al.* (1993a) modeled the residual stresses induced by cool down of a metal matrix periodic fiber monolayer from the processing temperature using a micromechanical analysis. The matrix was modeled by Miller's (1987) unified thermoviscoplastic constitutive theory. Spatially uniform temperature distribution was assumed, since relatively slow cooling rates were considered. Results obtained by the above authors have demonstrated that matrix thermoviscoplasticity can be significant during cooling down. Non-uniform temperature distribution was assumed in their other work [see e.g. Jeong *et al.* (1993b)].

Quite recently, Eggleston and Krempl (1992) studied the transverse creep behavior of titanium-based metal matrix composites. Comparing with experimental results, they found that a perfectly bonded interface model always underpredicted the creep behavior of the composite and that interface between the fiber and the matrix debonded during composite deformation. Also, they emphasized that residual stresses are one of the primary mechanisms for keeping the interface between the fiber and the matrix intact. They have also implemented various interface models to approximate the test data for both transverse creep and tensile loading [see e.g. Eggleston and Krempl (1993)].

Although considerable research has appeared recently, the current authors have found no results in the open literature which address the issues of thermal spatial gradients and

viscoplasticity in continuous fiber MMCs. Such an analysis is discussed in the body of this paper.

2. FORMULATION

The problem of interest in this work is to model the behavior of a single ply metal matrix composite subjected to cool down from the processing temperature, as shown in Fig. 1. When a metal matrix composite is cooled down from the processing temperature to room temperature, it is normally assumed that the temperature is spatially uniform in the RVE. However, rapid cooling rates may cause non-uniform temperature distributions which can induce significantly different stress distributions. Thus, an in-house heat transfer code is utilized herein to obtain residual stresses due to the non-uniform temperature distribution after cooling down from the processing temperature. Mechanical loading is subsequently applied to the RVE in order to obtain the average stress vs average strain response of the composite. The following subsections will describe the formulation of the thermal and mechanical solution schemes.

2.1. *Governing equations*

The composite RVE is shown in Fig. 1. The displacement vector field $u_i(x_j, t)$ and the temperature field $T(x_j, t)$ are chosen as the primary field variables. The Cauchy stress tensor σ_{ij} and the infinitesimal strain tensor ε_{ij} are chosen as the secondary field variables. The standard range and summation conventions apply to all subscripts in these equations, unless otherwise noted. The governing equations for the composite micromechanics problem consist of the mathematical statements of the conservation of momentum, conservation of energy, kinematical constraints, constitutive equations which describe the thermomechanical response of each material phase, and boundary conditions. These are:

(a) *Conservation of momentum.*

$$\sigma_{ji,j} = 0. \tag{1}$$

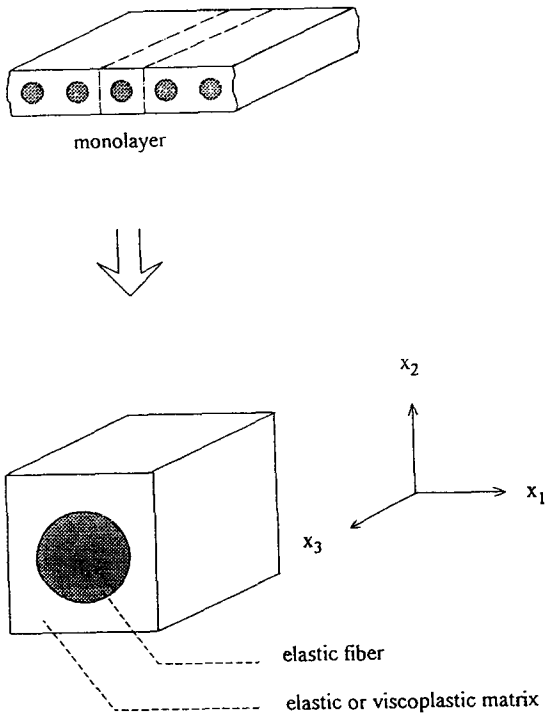

Fig. 1. Representative volume element of a periodic single layer composite (infinitely extended in the x_3-direction).

(b) *Conservation of energy.*

$$-q_{i,i} = \rho C_v \dot{T}, \tag{2}$$

where ρ is the mass density and C_v is the specific heat at constant volume. Note that the above equation assumes that mechanical coupling is negligible.

(c) *Strain-displacement equation.*

$$\varepsilon_{ij} = \tfrac{1}{2}(u_{i,j} + u_{j,i}). \tag{3}$$

(d) *Mechanical constitutive equations.* The fiber phase in this problem is characterized as isotropic linear thermoelastic, given by

$$\sigma_{ij} = C^{f}_{ijkl}(\varepsilon_{kl} - \varepsilon^{T}_{kl}), \tag{4}$$

where C^{f}_{ijkl} represents the isotropic elastic modulus tensor for the fiber phase and ε^{T}_{kl} is the thermal strain.

The thermoviscoplastic constitution of the matrix phase is substantially more difficult to characterize. Of the unified thermoviscoplasticity constitutive theories currently available [see e.g. Miller (1987)], the model due to Bodner (1987) was chosen for this analysis because of its versatility in modeling many different inelastic phenomena. Since a detailed explanation of this complex constitutive theory is beyond the scope of this paper, the model is simply summarized below.

In Bodner's unified constitutive theory, the stress–strain relation is given in rate form by

$$\dot{\sigma}_{ij} = C^{m}_{ijkl}(\dot{\varepsilon}_{kl} - \dot{\varepsilon}^{I}_{kl} - \dot{\varepsilon}^{T}_{kl}), \tag{5}$$

where C^{m}_{ijkl} is the matrix elastic modulus tensor, ε_{ij} represents the total strain tensor, ε^{I}_{ij} is the inelastic strain tensor and ε^{T}_{ij} is the thermal strain tensor. The following set of equations serves to predict the growth of ε^{I}_{ij} during cool down from the processing temperature:

$$\dot{\varepsilon}^{I}_{ij} = \dot{\lambda}\sigma'_{ij}; \quad \sigma'_{ij} = \sigma_{ij} - \tfrac{1}{3}\delta_{ij}\sigma_{kk}. \tag{6}$$

The kinetic equation for the effective inelastic strain rate is given by

$$D^{I}_{2} = (D_0)\exp\left[-\left(\frac{Z^2}{3J_2}\right)^{n}\right] \tag{7}$$

with

$$D^{I}_{2} = \tfrac{1}{2}\dot{\varepsilon}^{I}_{ij}\dot{\varepsilon}^{I}_{ij}; \quad J_2 = \tfrac{1}{2}\sigma'_{ij}\sigma'_{ij}, \tag{8}$$

whereas from eqn (6)

$$\dot{\lambda} = \left(\frac{D^{I}_{2}}{J_2}\right)^{1/2}. \tag{9}$$

The evolution equations of the hardening variables are given in the following:

$$\dot{Z} = m_1(Z_1 - Z)\dot{W}_1 - A_1 Z_1 \left(\frac{Z - Z_2}{Z_1}\right)^{r_1} \tag{10}$$

with

$$Z(0) = Z_0; \quad \dot{W}_1 = \sigma_{ij}\dot{\varepsilon}^1_{ij}. \tag{11}$$

The quantities D_0, n, m_1, Z_0, Z_1, Z_2, A_1 and r_1 appearing in eqns (7)–(11) are material constants. Several procedures exist for constructing these constants from experimental data [see e.g. Bodner (1987); Chan *et al.* (1988); James *et al.* (1987)]. Although an anisotropic hardening form exists for Bodner's model, it was not used herein because the material properties were not available for Ti-15-3.

(e) *Thermal constitutive equations.* For both fiber and matrix we assume that the Fourier law of heat conduction holds:

$$q_i = -kT_{,i}, \tag{12}$$

where k is the coefficient of thermal conductivity in isotropic media. Note that k may be a function of temperature, so that eqn (12) is nonlinear.

(f) *Boundary conditions.* Conditions imposed on the field variables at the boundary of the domain of interest, S, are also necessary. The Dirichlet mechanical boundary conditions are given by

$$u_i = \hat{u}_i \text{ on } S_1. \tag{13}$$

Neumann mechanical boundary conditions are given by

$$T_i = \sigma_{ji} n_j = \hat{T}_i \text{ on } S_2, \tag{14}$$

where $S_1 \cup S_2 = S$. Dirichlet thermal boundary conditions are

$$T = \hat{T} \text{ on } S_1^{\mathrm{T}}. \tag{15}$$

Neumann thermal boundary conditions are

$$q_i n_i = \hat{q}_n \text{ on } S_2^{\mathrm{T}}, \tag{16}$$

where $S_1^{\mathrm{T}} \cup S_2^{\mathrm{T}} = S$. Note that the symbol $\hat{}$ indicates known quantities which are prescribed over the entire time scale.

2.2. *Variational formulation and finite element implementation*

In this section, the first part describes the incremental finite element formulation for mechanical analysis by starting with the variational formulation for the equilibrium equation. The second part outlines the finite element formulation for thermal analysis by starting with the variational formulation for the heat conduction equation. Numerical schemes to solve these equations are elucidated.

2.2.1. *Conservation of momentum.* Equation (1) must be cast in a variational formulation. Integrating eqn (1) against a variation δu_i over the volume Ω, and then integrating by parts results in (Reddy, 1993)

$$\int_\Omega \sigma_{ij}\delta u_{i,j}\,\mathrm{d}\Omega = \int_S T_i \delta u_i\,\mathrm{d}S. \tag{17}$$

Equation (17) is the virtual work equation for the case of negligible accelerations and body forces.

Incrementalization of eqn (17) and introduction of eqns (3), (4) and (5) will result in a nonlinear variational principle which can be discretized by the finite element method. This formulation is detailed in Jeong (1993). This procedure has been utilized to develop the in-house code SADISTIC (Structural Analysis of Damage Induced Stresses in Thermo-Inelastic Composites). This algorithm requires extensive computational requirements due to the time stepping algorithm necessary for integrating the viscoplastic constitutive equations mentioned in Section 2.1(d). Further discussion of this issue is contained in Allen *et al.* (1993).

2.2.2. *Conservation of energy.* Equations (2) and (12) govern the heat conduction for isotropic solids. In the context of a variational formulation, one multiplies eqn (2) by a variation δT, substitutes constitutive eqn (12) and integrates all terms over the domain Ω. Subsequent integration by parts will give [see e.g. Reddy (1993)]

$$\int_\Omega \left[\rho C_v \frac{\partial T}{\partial t} \delta T + k T_{,i} (\delta T)_{,i} \right] d\Omega + \int_S q_i n_i \delta T \, dS = 0. \tag{18}$$

To spatially approximate eqn (18), the entire domain is first discretized into n_e elements with n_d nodes each. A set of functions N_i is chosen to spatially interpolate the temperature within each element

$$T(x_k, t) = \sum_{i=1}^{n_d} N_i(x_k) T_i(t), \tag{19}$$

where N_i are the shape functions and T_i is a set of temporal functions equivalent to element nodal temperatures. Substituting eqn (19) into eqn (18) finally gives the following global equations:

$$C_{ij} \dot{T}_j + K^{\mathrm{T}}_{ij} T_j = R^{\mathrm{T}}_i, \tag{20}$$

where the superscript T refers to thermal analysis. C_{ij}, K^{T}_{ij}, and R^{T}_i are matrices of thermal capacitance, thermal conductance and the thermal load vector, respectively, and they are defined in the Appendix. Further discussion of the solution of eqn (20) is also given in the Appendix.

2.3. *Meshes and boundary conditions*

2.3.1. *Meshes.* The RVE for the periodic continuous fiber composite shown in Fig. 1 can be further subdivided into quarters by taking advantage of the geometric and loading symmetry, as shown in Fig. 2. Assuming plane strain conditions in the x_3-direction and heat conduction in the x_1–x_2 plane, the two-dimensional domain shown in Fig. 2 is sufficient. The element type chosen for this analysis is the constant strain triangle. Because of the material nonlinearity and geometric irregularity of the problem at hand, a relatively dense mesh is required to achieve a realistic solution. Convergence studies were performed using the meshes shown in Fig. 2. When the temperature is spatially non-uniform, the meshes with less than 618 elements were not refined enough to capture the thermal gradient. The RVE and converged finite element mesh are shown in Fig. 3. This mesh has 340 nodes and 618 constant strain triangle elements.

2.3.2. *Boundary conditions.* The mechanical and thermal boundary conditions are shown in Fig. 3. The multiple constraint condition on the right face is satisfied by use of a penalty function [see e.g. Cook *et al.* (1989)]. Note that a spatially uniform temperature history is prescribed on the free surface, while all other faces of the RVE are considered to be adiabatic boundaries with zero heat flux across them due to symmetry.

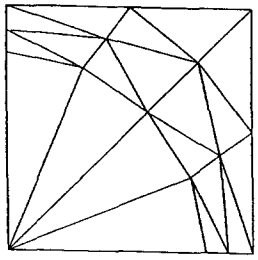

16 NODES, 20 CST'S

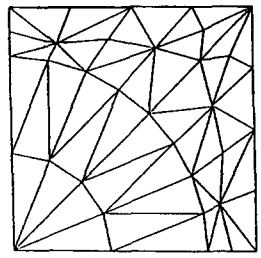

35 NODES, 52 CST'S

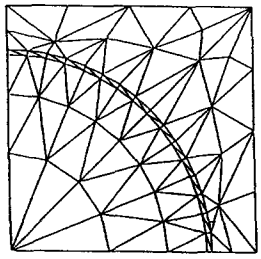

69 NODES, 116 CST'S

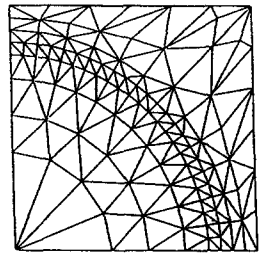

117 NODES, 204 CST'S

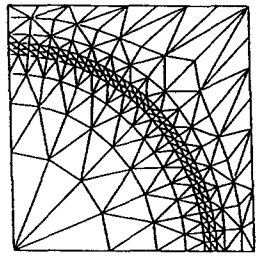

182 NODES, 328 CST'S

Fig. 2. Several meshes used in both mechanical and thermal analyses.

3. DISCUSSION OF MODEL PREDICTIONS

In this section, some results from the finite element program are examined. The material system selected for this analysis is Ti-15-3 matrix reinforced with continuous fiber SCS-6 silicon carbide fibers of diameter 140 μm in a single ply. A fiber volume fraction of 0.5 was selected. Thermoelastic material properties for the fiber and matrix phases are shown in Table 1 [see e.g. MIL Handbook-5C (1976)]. Temperature dependent material properties are linearly interpolated in the code. Thermoviscoplastic material constants for Bodner's model are shown in Table 2 (Imbrie, 1992). We should note that the directional hardening parameter Z_D is not included in the analysis since the material constants are not available. The analysis was performed assuming a stress-free initial processing temperature of 815°C.

3.1. *Thermoelastic results*

To investigate the effects of different cooling rates, the thermoelastic problem is considered first. The Ti-15-3 matrix is assumed to be linear thermoelastic with material parameters taken from Table 1. Figure 4(a) shows the temperature history for slow cooling rates at two points; point A is at the center of the fiber and the exterior point B is on the free surface. Due to the small thickness of the unit cell (87.7 microns) and the large thermal diffusivity of the matrix, for slow cooling rates the temperature is almost the same at points A and B. However, as the cooling rates become larger, the temperature difference between these two points becomes more prominent, as can be seen in Fig. 4(b).

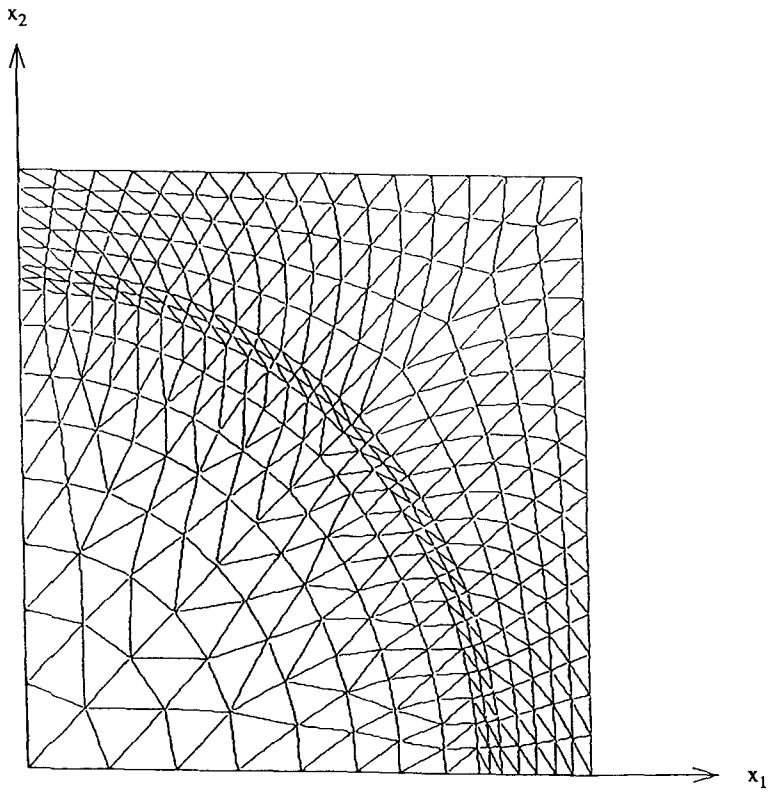

Fig. 3. 618 element mesh and thermomechanical boundary conditions (two-dimensional).

The effect of spatial temperature gradients on stresses is illustrated in Fig. 5. In these thermoelastic results, the in-plane matrix stresses are plotted as functions of time at the interior point C along the x_1-axis at the fiber–matrix interface. Figure 5 shows that, if it is assumed that the temperature is spatially homogeneous during cool down, the predicted stresses are erroneous until steady state is reached. In fact, the spatially variable temperature predictions result in much higher peak compressive radial stresses during rapid cool down.

The thermoelastic in-plane matrix residual stresses at the interface are shown in Fig. 6 for various cooling rates, where the interface angle is defined to be positive counterclockwise from the horizontal axis. In addition, the stress components are shown at the end of cooling from the processing temperature of 815°C to room temperature (23°C) for each of the cooling rates, as well as at a time of 150 minutes, which has been found to be the time at which steady state is reached for the slowest cooling rate. Since all other cases reach steady state more rapidly, at this time the stress field along the interface is the same for the four different cooling rates because the temperature field becomes spatially uniform and the thermoelastic solution is independent of the thermal loading path.

Figure 6 shows that for a large part of the interface, the radial and shear components of the in-plane matrix stresses at the interface exceed their long time asymptotic values, which correspond to spatially uniform temperature in the RVE. This overshoot is maximized at interface points farthest away from the free surface [at zero degrees interface angle for the radial stress, Fig. 6(a)] due to the delay in the cooling of the fiber with respect to the cooling of the matrix. In Fig. 6(a) the overshoot occurs from 0° to about 30°, where spatial inhomogeneity in temperature substantially increases the thermal stress build-up due to the mismatch in the thermal expansion coefficients of the two phases. As shown in Fig. 6(b), the hoop stress is lowest for the most rapid cooling rates, so that radial cracking is not expected to be affected by the cooling rate. Note also that the overshoot in the shear stress occurs at some intermediate angles and diminishes as the maximum interface angle is approached [Fig. 6(c)]. An accurate prediction of the spatial and time dependence of the interface shear stress is extremely important since interface failure may be initiated in shear.

Table 1. Thermoelastic properties of matrix and fiber (Jeong, 1993)

Matrix: Ti-15-3	
Elastic modulus (E^M) (MPa)	97,812 (at 23°C) 61,166 (at 649°C) 51,781 (at 815°C)
Poisson's ratio (ν^m)	0.32
Thermal expansion coefficient (α^m) (/°C)	8.73×10^{-6} (at 23°C) 9.0×10^{-6} (at 93°C) 9.36×10^{-6} (at 204°C) 9.65×10^{-6} (at 315°C) 9.90×10^{-6} (at 427°C) 10.13×10^{-6} (at 538°C) 10.26×10^{-6} (at 649°C) 10.26×10^{-6} (at 871°C)
Thermal Conductivity (k^m) $\left(\frac{J}{s-m-°C}\right)$	7.27 (at 23°C) 7.27 (at 93°C) 8.56 (at 204°C) 9.89 (at 315°C) 13.83 (at 649°C) 15.08 (at 760°C) 16.12 (at 871°C)
Specific Heat (C_p^m) $\left(\frac{J}{kg-°C}\right)$	514.97 (at 23°C) 544.31 (at 93°C) 795.54 (at 649°C) 858.31 (at 760°C) 921.15 (at 871°C)
Density (ρ^m) (kg/m^3)	4428.43
Fiber: SCS-6 Silicon Carbide	
Elastic modulus (E^f) (GPa)	394
Poisson's ratio (ν^f)	0.25
Thermal expansion coefficient (α^f) (/°C)	4.86×10^{-6}
Thermal Conductivity (k^f) $\left(\frac{J}{s-m-°C}\right)$	138.06
Specific Heat (C_v^f) $\left(\frac{J}{kg-°C}\right)$	835.63
Density (ρ^f) (kg/m^3)	3099

Table 2. Material constants for Bodner's model (Imbrie, 1992)

Ti-15-3

1. Temperature independent constants
   $D_0 = 1.0 \times 10^4$/sec
   $Z_1 = 1172$ MPa
   $Z_3 = 0$ MPa
   $r_1 = 1$
   $m_1 = 0.2466$/MPa

2. Temperature dependent constants

Constants	Units	23°C	483°C	566°C	649°C	815°C
n		7.0	5.0	3.5	3.0	2.5
Z_0	MPa	965	827	689	621	553
Z_2	MPa	965	827	689	621	553
A_1	/sec	0	0	0	0	0

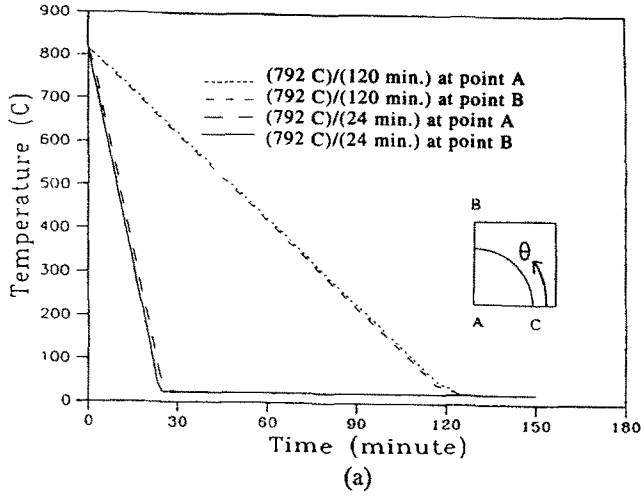

Fig. 4. Effect of heating rate on temperature at points A and B.

3.2. *Viscoplastic results*

The remainder of the results reported herein emphasize the importance of matrix viscoplasticity. Figure 7 shows the variation of radial and hoop stress with time at point C. As shown in Fig. 7(a), a larger overshoot in the radial stress occurs in the rapid cooling case. This may result in a smaller permanent residual radial stress at the end of cooling due to increased inelasticity. Once again, no deleterious effects are seen in the hoop stress, as shown in Fig. 7(b). Note that the steady state solution is different for the two different cooling rates, due to the path and rate dependence of the viscoplastic matrix.

In Fig. 8, matrix stresses at the fiber–matrix interface are shown at two different times for the rapid cooling rate of 792°C/1.2 minutes. At this cooling rate, steady state is reached after approximately 7.5 minutes. A comparison of Figs 6 and 8 indicates that the steady state matrix stresses predicted by the viscoplastic analysis are significantly different from those predicted by the thermoelastic analysis. In particular, the maximum radial stresses are reduced by at least 30% and the hoop stresses are reduced by at least 20%, while the shear stresses are nearly identical.

In Fig. 9, it is also found that viscoplasticity significantly decreases the predicted matrix stresses at point C when compared to thermoelastic predictions. It is thus suggested by these results that thermoelastic analyses are quite conservative when predicting fiber and radial matrix cracking, as well as interface fracture.

Finally, the matrix stresses along the fiber–matrix interface for both the elastic and viscoplastic matrix cases are shown in Fig. 10. As shown in Figs 10(a, b), the maximum

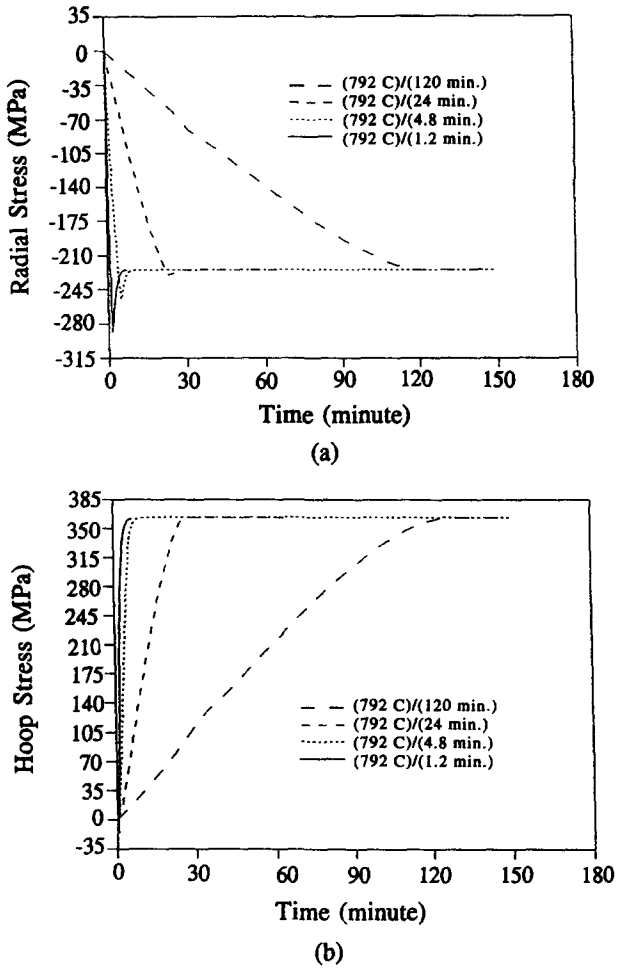

Fig. 5. Matrix stresses at interior point C of the fiber–matrix interface for various cooling rates for elastic matrix and non-uniform temperature distribution.

deviation of hoop and radial stresses is observed at the interface angle zero. The shear stresses at the interface do not appear to be strongly affected by matrix viscoplasticity, as shown in Fig. 10(c).

3.3. *Mechanical loading with/without residual stresses*

In this section, the effect of mechanical loading is considered. Two cases are studied; one for which mechanical loading is applied at room temperature, and a second for which mechanical loading is applied after reheating to an operating temperature of 483°C, as shown in Fig. 11. The absolute value of the heating rate is assumed to be the same as the cooling rate. A moderate cooling rate of 792°C/24 minutes is chosen for this analysis. Temperature distributions at room temperature and at operating temperature are shown in Fig. 12.

Figure 13 shows the von Mises effective stresses ($\sqrt{3J_2}$) for room and operating temperatures. Effective stress is used in eqn (7) to obtain the inelastic strain rate. From Table 2, it can be seen that the initial value, Z_0, of the internal variable Z at room temperature is 140 ksi (965 MPa), thus indicating that a significant portion of the matrix has already yielded at room temperature, as shown in Fig. 13(a). On the other hand, at the operating temperature, as shown in Fig. 13(b), the effective stress is well below Z_0, which at this temperature is 120 ksi (827 MPa).

We will now endeavor to determine how the effective uniaxial mechanical behavior is affected by the residual stresses under various conditions. In Figs 14 and 15, average stress–strain curves are given. As shown in both figures, if the residual stresses due to cool

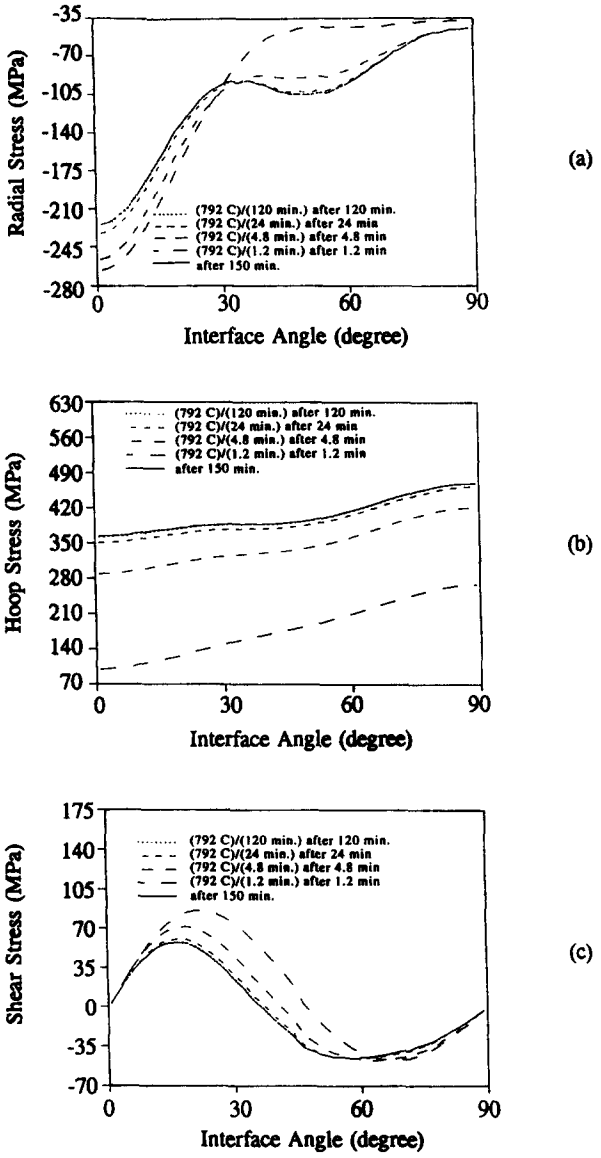

Fig. 6. Matrix stresses at the fiber–matrix interface for various cooling rates assuming thermoelastic cool down and non-uniform temperature distribution.

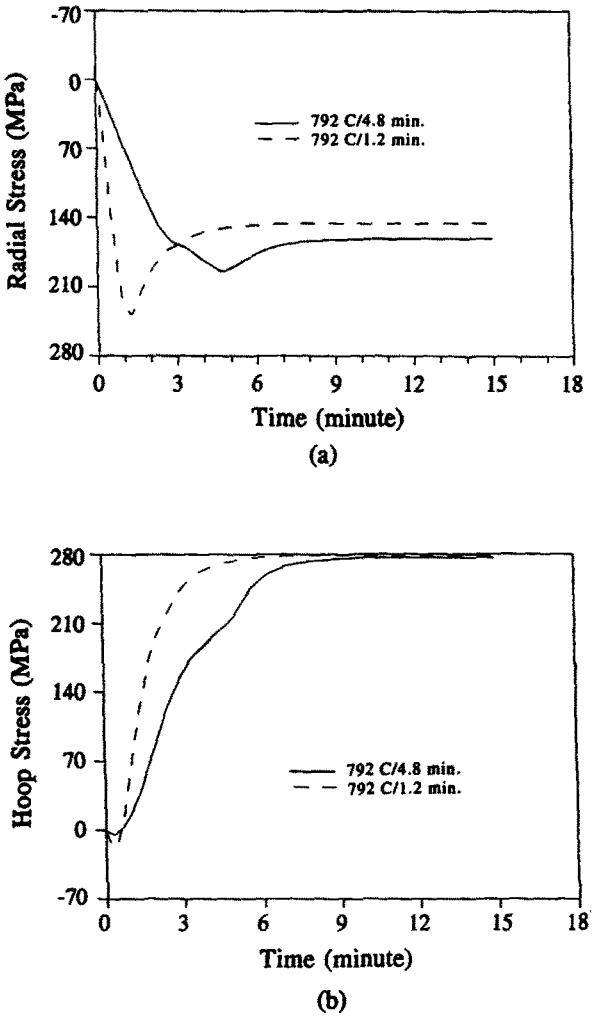

Fig. 7. Interface stresses at point C for various cooling rates assuming viscoplastic matrix and non-uniform temperature distribution.

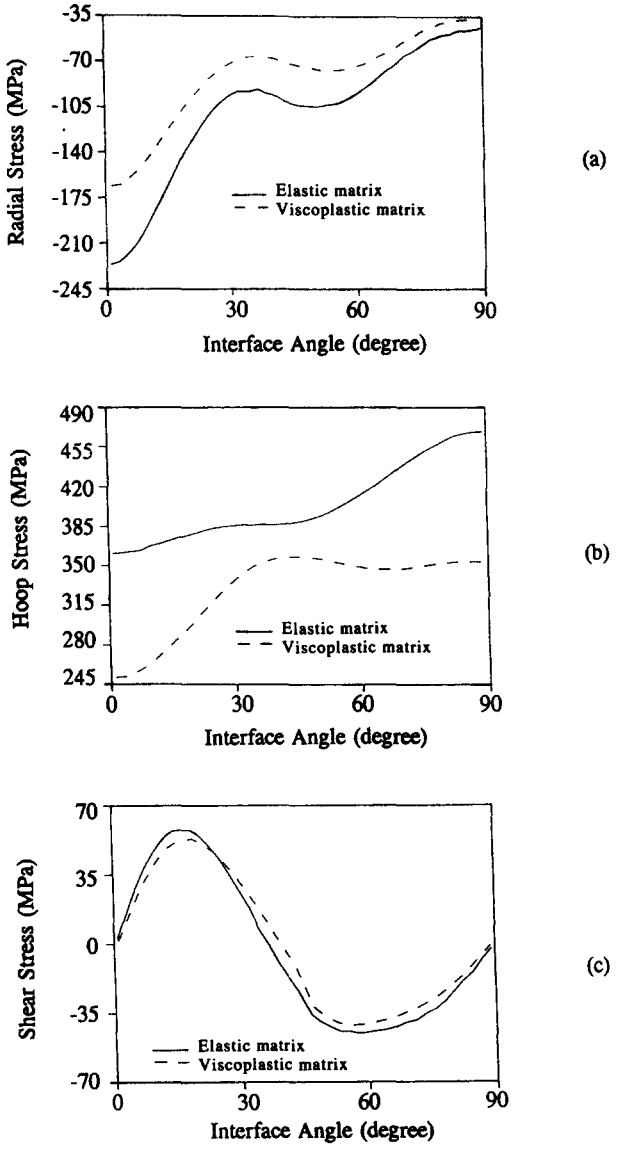

Fig. 8. Effect of matrix viscoplasticity on predicted stresses under non-uniform temperature, cooling rate 792°C/120 min.

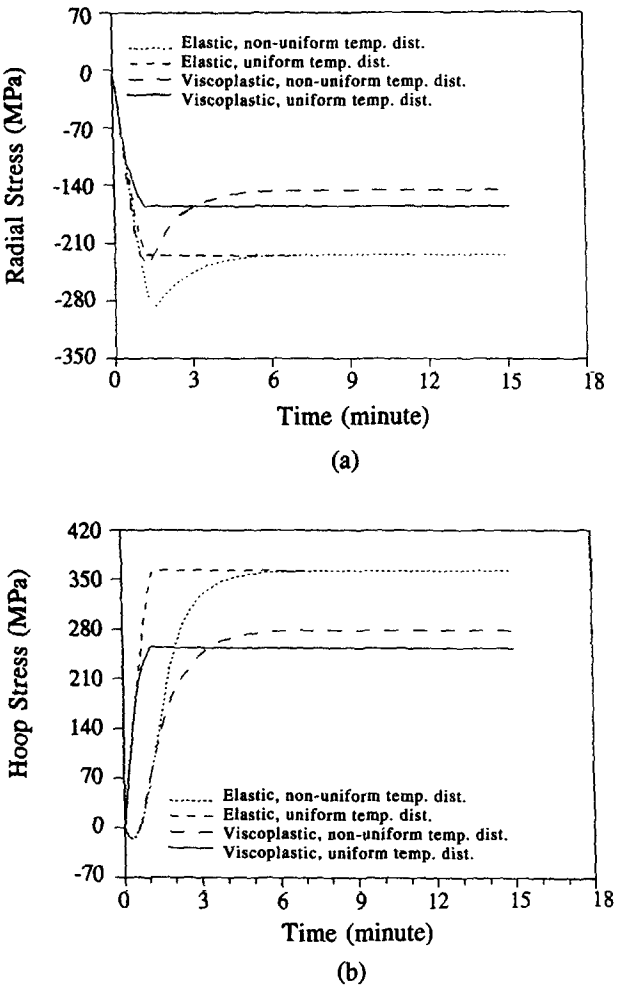

Fig. 9. Effect of matrix viscoplasticity and thermal gradients on predicted stresses at point C for rapid cooling rate, 792°C/1.2 min.

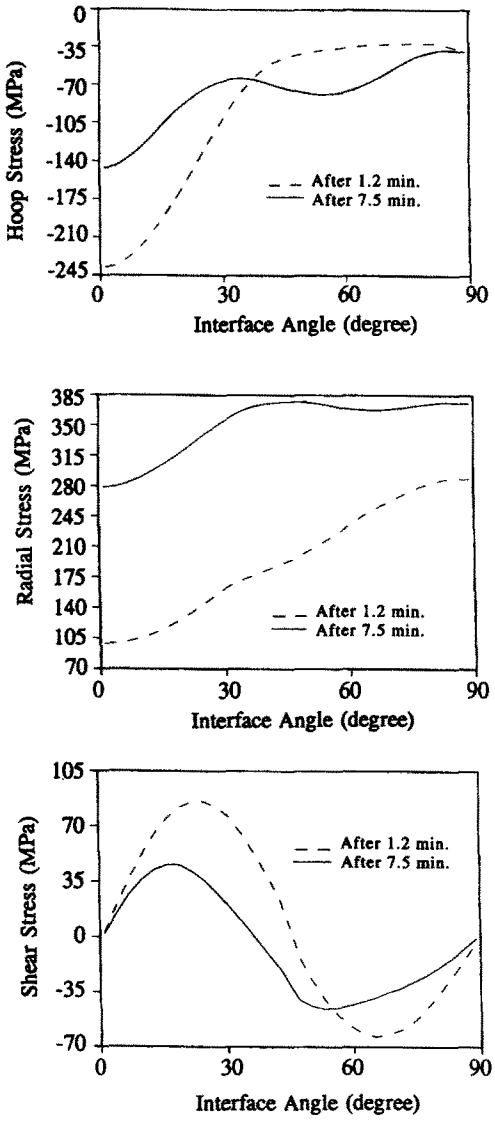

Fig. 10. Effect of matrix viscoplasticity on predicted stresses under non-uniform temperature, cooling rate 792°C/1.2 min.

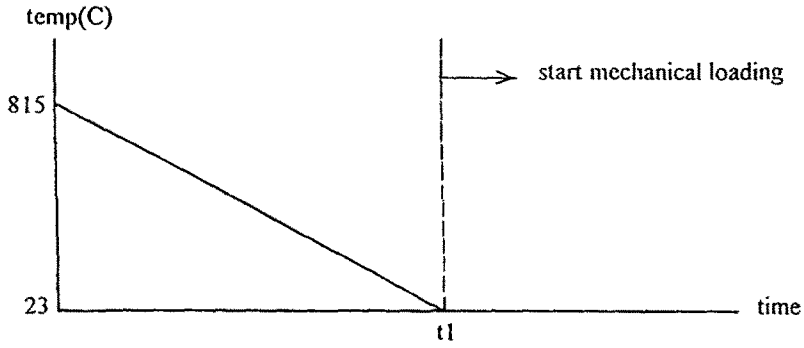

(a) mechanical loading is applied at time t_1

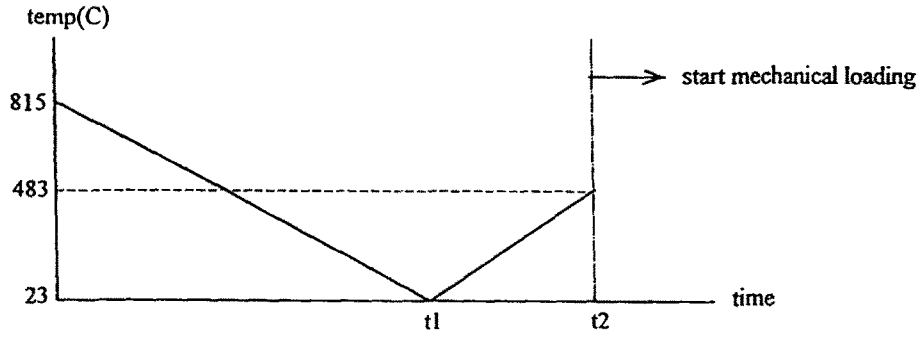

(b) mechanical loading is applied at time t_2

Fig. 11. Mechanical loadings applied at room temperature and at operating temperature.

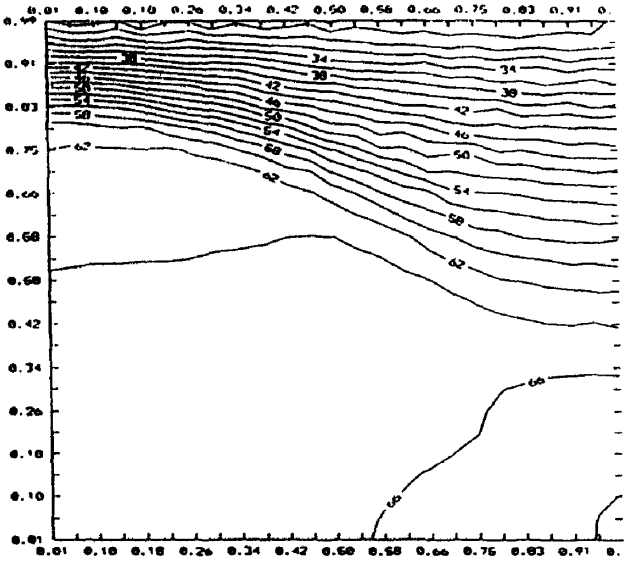

(a) at room temperature (after 24 min.)

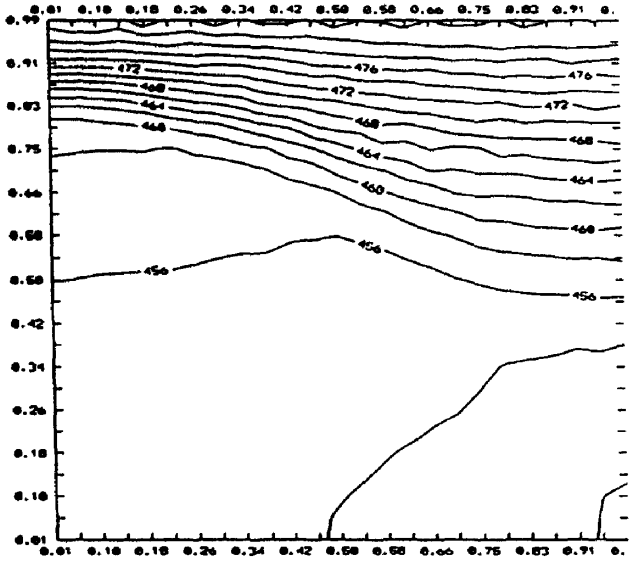

(b) at operating temperature (after 38 min.)

Fig. 12. Temperature distribution at room temperature and at operating temperature.

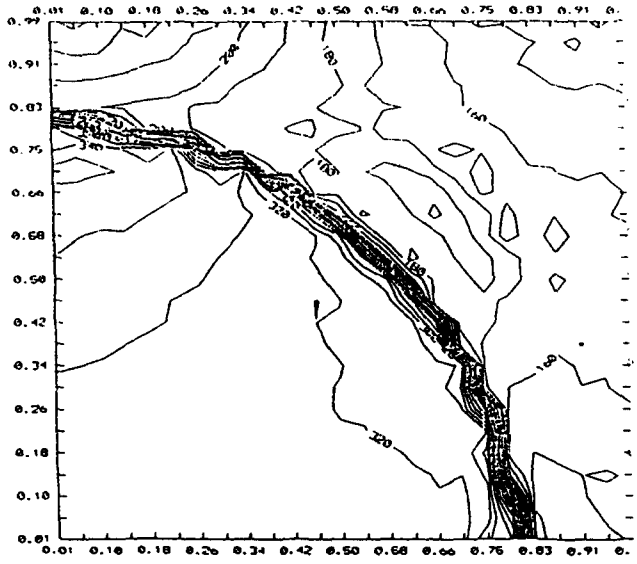

(a) at room temperature

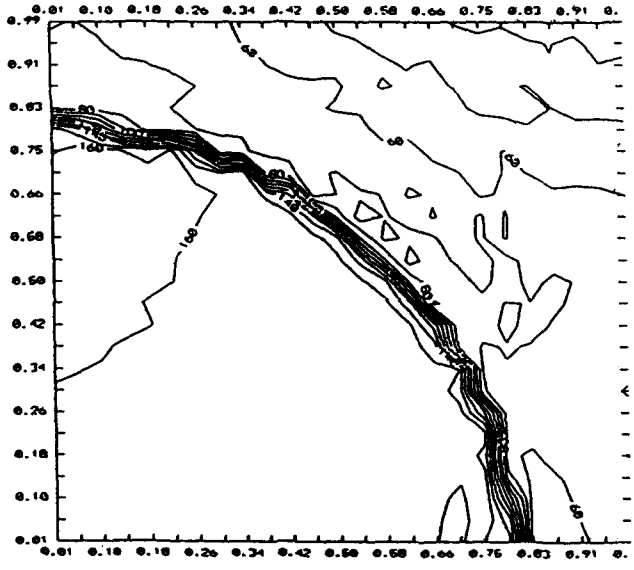

(b) at operating temperature

Fig. 13. Von Mises effective stresses at room temperature and operating temperature at cooling rate, 792°C/24 min (non-uniform temperature distribution and plane strain are assumed).

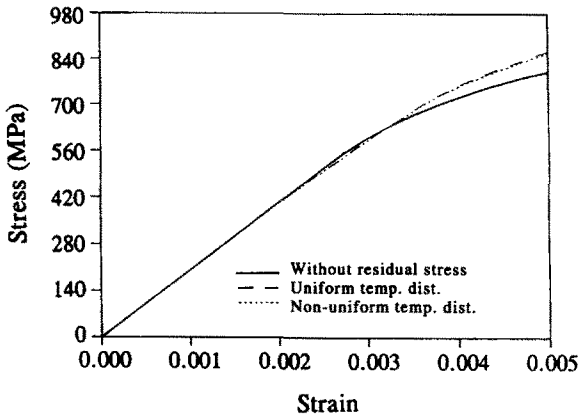

Fig. 14. Effect of residual stress on transverse stress–strain behavior of the composite at room temperature.

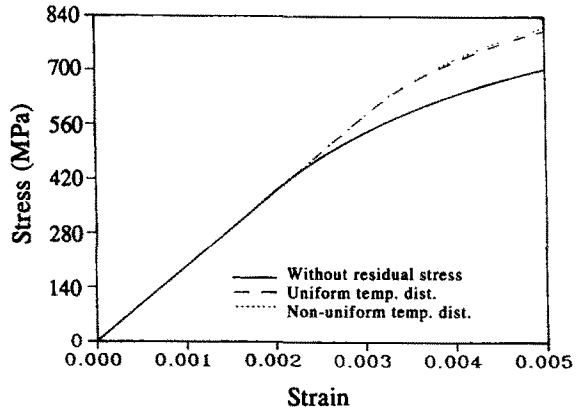

Fig. 15. Effect of residual stress on transverse stress–strain behavior of the composite at operating temperature.

down are not included, the effective stress–strain behavior is underpredicted both at room temperature and the operating temperature. This suggests that residual stresses may also affect the interface stresses. To see this, consider Figs 16, 17 and 18. Figure 16 shows the interface stresses caused by mechanical loading, but neglecting the residual stresses caused by thermal cool down and subsequent heating to the operating temperature. Figure 17, on the other hand, accounts for the residual stresses, but the mechanical loading is applied at room temperature. Finally, Fig. 18 shows the interface stresses when the mechanical load is applied at the operating temperature and residual stresses are included. It is obvious from a comparison of the figures that the interface stresses are not accurately predicted when the thermal residual stresses are not included in the analysis. Furthermore, experimental evidence [see e.g. Jansson *et al.* (1991)] indicates that the interface bond is primarily due to thermal residual stresses. Therefore, since the radial stresses shown in Fig. 15 are tensile, the results without residual stresses shown in this figure are fallacious.

On the other hand, it is also clear from a comparison of Figs 17 and 18 that the operating temperature causes the thermal residual stresses to be relieved during reheating. Therefore mechanical loading induces tensile radial stresses (and subsequent interface debonding) at lower mechanical strains than at room temperature. Alternatively, the hoop stress is lower at the operating temperature, indicating that radial cracking in the matrix is more likely when mechanical loading is applied at room temperature.

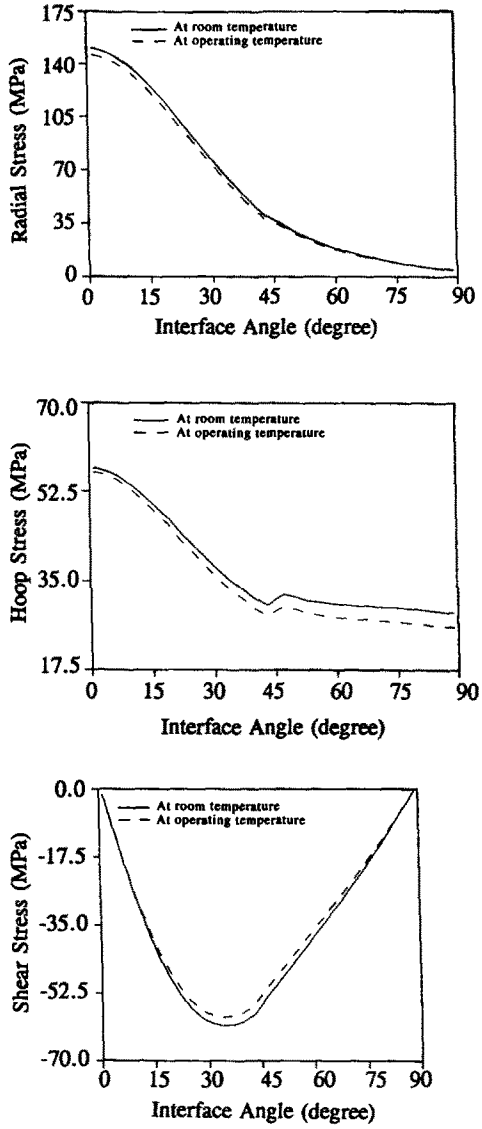

Fig. 16. Matrix stresses along the fiber–matrix interface due to mechanical loading without residual stresses at average strain = 0.0005.

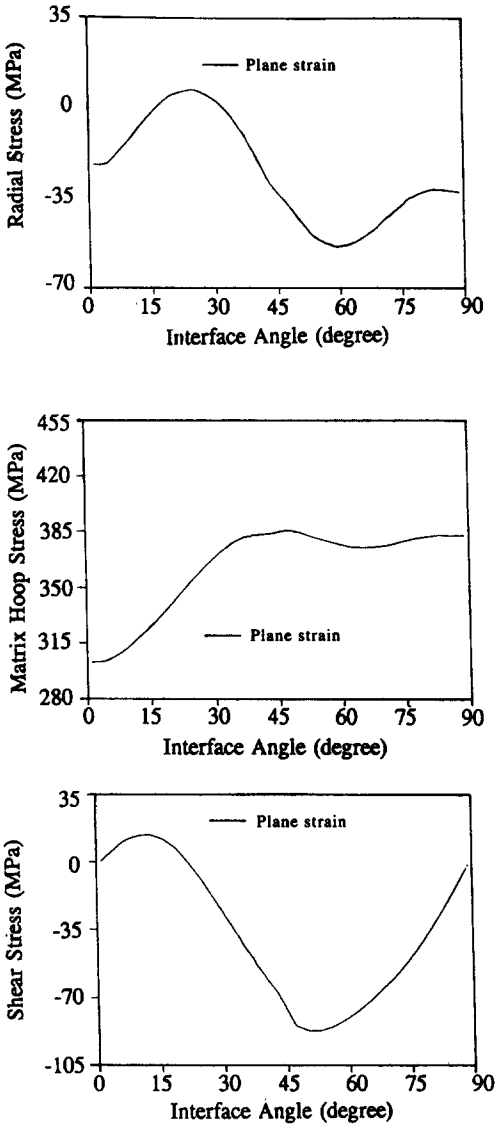

Fig. 17. Interface stresses due to mechanical loading with residual stresses at room temperature and at average strain = 0.0005.

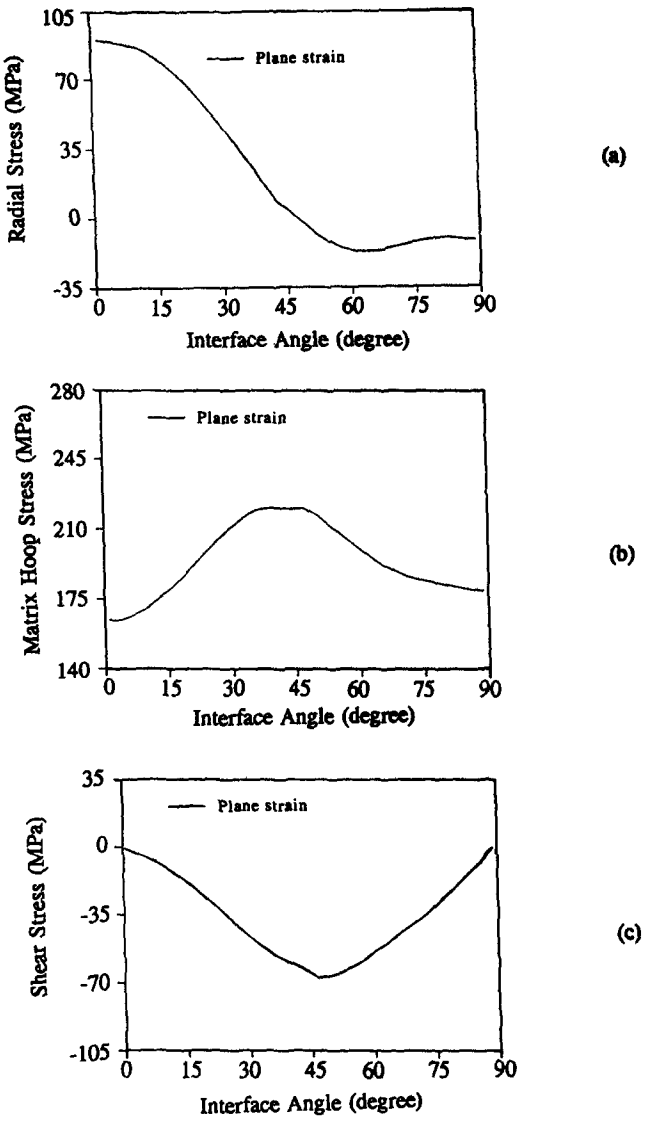

Fig. 18. Interface stresses due to mechanical loading with residual stresses at operating temperature and at average strain = 0.0005.

4. SUMMARY AND CONCLUSION

Residual stresses in the RVE (representative volume element) of a monolayer metal matrix composite have been studied. Various cooling rates together with uniform–non-uniform temperature distribution, elastic–viscoplastic matrix have been considered. The major results are:

1. Non-uniform temperature distribution should be taken into account when rapid cool down is performed since the short time radial and shear components of the in-plane matrix stresses at the interface exceed their long time asymptotic values.

2. Contrary to the results reported by other reseachers [see e.g. Jansson *et al.* (1991)], significant inelasticity occurs in the matrix during cool down, thereby significantly decreasing the matrix stresses, and in particular, the interface stresses, when compared to thermoelastic results at room temperature.

3. When mechanical loading is applied, interface stresses are strongly influenced by the presence of the thermal residual stresses. Thus, spatial temperature variations and matrix viscoplasticity may be important in predicting the onset of fiber, interface and matrix cracking.

REFERENCES

Aboudi, J. (1980). Elastoplasticity theory for composite materials. *Solid Mech. Archives* **11,** 141–183.

Allen, D. H., Jones, R. H. and Boyd, J. G. (1993). Micromechanical analysis of a continuous fiber metal matrix composite including the effects of matrix viscoplasticity and evolving damage. *J. Mech. Phys. Solids*, in press.

Bahei-El-Din, Y. A. and Dvorak, G. J. (1991). Local fields in uncoated and coated high temperature fibrous composite systems. In *Damage and Oxidation Protection in High Temperature Composites—Vol. 2*, AD-Vol. 25-2, pp. 21–34. ASME, New York.

Benveniste, Y. (1985). The effective mechanical behavior of composite materials with imperfect contact between the constituents. *Mech. Mater.* **4,** 197.

Bodner, S. R. (1987). Review of a unified elastic–viscoplastic theory. In *Unified Constitutive Equations for Creep and Plasticity* (Edited by A. K. Miller). Elsevier Science, New York.

Chan, K. S., Bodner, S. R. and Lindholm, U. S. (1988). Phenomenological modeling of hardening and thermal recovery in metals. *J. Engng Mater. Tech.* **110,** 1–8.

Cook, R. D., Malkus, D. S. and Plesha, M. E. (1989). *Concepts and Applications of Finite Element Analysis*, 3rd edition. John Wiley and Sons, New York.

Eggleston, M. R. and Krempl, E. (1992). Modeling the transverse creep of titanium-based metal matrix composites. In *Damage Mechanics in Composites*, AMD-Vol. 150/AD-Vol. 32, pp. 313–326. ASME, New York.

Eggleston, M. R. and Krempl, E. (1993). The effect of the fiber–matrix interface on the transverse creep of SCS-6/Ti-6Al-4V. 1st ASCE-ASME-SES Joint Meeting.

Herakovich, C. T., Aboudi, J. and Beuth, J. L., Jr (1990). A micromechanical composite yield model accounting for residual stresses. *Proc. IUTAM Symp. Inelastic Deformation of Composite Materials* (Edited by G. J. Dvorak), pp. 373–387. Springer-Verlag, Berlin.

Imbrie, P. K. (1992). Personal communication. Aerospace Engineering Department, Texas A and M University.

James, G. H., Imbrie, P. K., Hill, P. S., Allen, D. H. and Haisler, W. E. (1987). An experimental comparison of current viscoplastic models at elevated temperature. *J. Engng Mater. Tech.* **109,** 130–139.

Jansson, S., Deve, H. E. and Evans, A. G. (1991). The anisotropic mechanical properties of a Ti matrix composite reinforced with SiC fibers. *Metall. Trans. A.* **22,** 1991–2975.

Jeong, G. S. (1993). Residual stress development due to cool down in viscoplastic metal matrix composites. Ph.D. Dissertation, Aerospace Engineering Department, Texas A and M University.

Jeong, G. S., Jones, R. H. and Allen, D. H. (1993a). Analysis of residual induced by cool down in viscoplastic metal matrix composites. In *Damage in Composite Materials* (Edited by G. Z. Voyiadjis), pp. 235–247. Elsevier Science, Amsterdam.

Jeong, G. S., Allen, D. H. and Lagoudas, D. C. (1993b). Residual stress evolution due to cool down in viscoplastic metal matrix composites. In *Thermomechanical Behavior of Advanced Structural Materials* (Edited by W. F. Jones), pp. 17–31. ASME, New York.

MIL-Handbook-5C (1976). Department of Defense.

Miller, A. K. (1987). *Unified Constitutive Equations for Creep and Plasticity*. Elsevier Science, Oxford.

Povirk, G. L., Needleman, A. and Nutt, S. R. (1991). An analysis of the effect of residual stresses on deformation and damage mechanisms in Al-SiC composites. *Mater. Sci. Engng A.* **132,** 31–38.

Reddy, J. N. (1993). *An Introduction to the Finite Element Method*, 2nd edition. McGraw-Hill, New York.

Sherwood, J. A. and Boyle, M. J. (1990). Investigation of the thermomechanical response of a titanium-aluminide/silicon-carbide composite using a unified state variable model and the finite element method. In *Microcracking-Induced Damage in Composites* (Edited by G. J. Dvorak and D. C. Lagoudas), Vol. 111, pp. 151–161. ASME, New York.

Sun, C. T., Chen, J. L., Sha, G. T. and Koop, W. E. (1990). Mechanical characterization of SCS/Ti-6-4 metal matrix composite. *J. Comp. Mater* **24,** 1029–1059.

Teply, J. L. and Dvorak, G. J. (1988). Bounds on overall instantaneous properties of elastic–plastic composites. *J. Mech. Phys. Solids* **36,** 29–58.

Wisnom, M. R. (1990). Factors affecting the transverse tensile strength of unidirectional continuous silicon carbide fiber reinforced 6061 aluminum. *J. Comp. Mater* **24,** 700–726.
Zywicz, E. and Parks, E. M. (1988). Thermo-viscoplastic residual stresses in metal matrix composites. *Comp. Sci. Tech.* **33,** 295–315.

APPENDIX

The thermal capacitance matrix is given by

$$C_{ij} = \sum_{e=1}^{n_e} \int_{\Omega_e} \rho C_v N_i N_j \, d\Omega. \tag{A1}$$

The thermal conductance matrix is given by

$$K_{ij}^T = \sum_{e=1}^{n_e} \int_{\Omega_e} (k N_{i,m} N_{j,m}) \, d\Omega. \tag{A2}$$

The load vector is given by

$$R_i^T = \int_S N_i q_n \, dS. \tag{A3}$$

Equations (20) and (A1)–(A3) complete the finite element discretization procedure. Imposition of boundary conditions is described in the MIL Handbook-5C (1976).

Various schemes have been reported to solve the heat transfer equations in time. The variable weighted method, which is also termed as Wilsom θ method elsewhere, approximates a weighted average of the derivative of temperature at two consecutive time steps by linear interpolation of the temperatures at the two time steps:

$$\theta \dot{T}_j^{t+\Delta t} + (1-\theta) \dot{T}_j^t = \frac{1}{\Delta T}(T_j^{t+\Delta t} - T_j^t), \tag{A4}$$

where θ is a weight factor ranging from 0 to 1. The Crank–Nicolson method which defines θ to be 0.5 is an unconditionally stable implicit scheme and is adopted in this formulation. Let $\theta = 0.5$ in eqn (A4) and substitute the result into eqn (20) to obtain

$$\bar{K}_{ij} T_j^{t+\Delta t} = \bar{R}_i^t, \tag{A5}$$

where

$$\bar{K}_{ij} = C_{ij} + \frac{\Delta t}{2} K_{ij}^T \tag{A6}$$

and

$$\bar{R}_i^t = \left(C_{ij} - \frac{\Delta t}{2} K_{ij}^T \right) T_j^t + \frac{\Delta t}{2} (R_i^{t+\Delta t} + R_i^t). \tag{A7}$$

The temperature field at time $t+\Delta t$ can be obtained by solving eqn (A5).